Biophys Rep 2018, 4(5):254–264
https://doi.org/10.1007/s41048-018-0071-1

Biophysics Reports

RESEARCH ARTICLE

Small-animal SPECT/CT imaging of cancer xenografts and pulmonary fibrosis using a ^{99m}Tc-labeled integrin αvβ6-targeting cyclic peptide with improved *in vivo* stability

Hao Liu[1], Liquan Gao[1], Xinhe Yu[1], Lijun Zhong[2], Jiyun Shi[3], Bing Jia[1,2], Nan Li[4], Zhaofei Liu[1]✉, Fan Wang[1,3]✉

[1] Medical Isotopes Research Center and Department of Radiation Medicine, School of Basic Medical Sciences, Peking University Health Science Center, Beijing 100191, China

[2] Medical and Healthy Analytical Center, Peking University, Beijing 100191, China

[3] Key Laboratory of Protein and Peptide Pharmaceuticals, CAS Center for Excellence in Biomacromolecules, Institute of Biophysics, Chinese Academy of Sciences, Beijing 100101, China

[4] Key Laboratory of Carcinogenesis and Translational Research (Ministry of Education/Beijing), Department of Nuclear Medicine, Peking University Cancer Hospital & Institute, Beijing 100142, China

Received: 24 May 2018 / Accepted: 17 July 2018 / Published online: 2 November 2018

Graphical Abstract

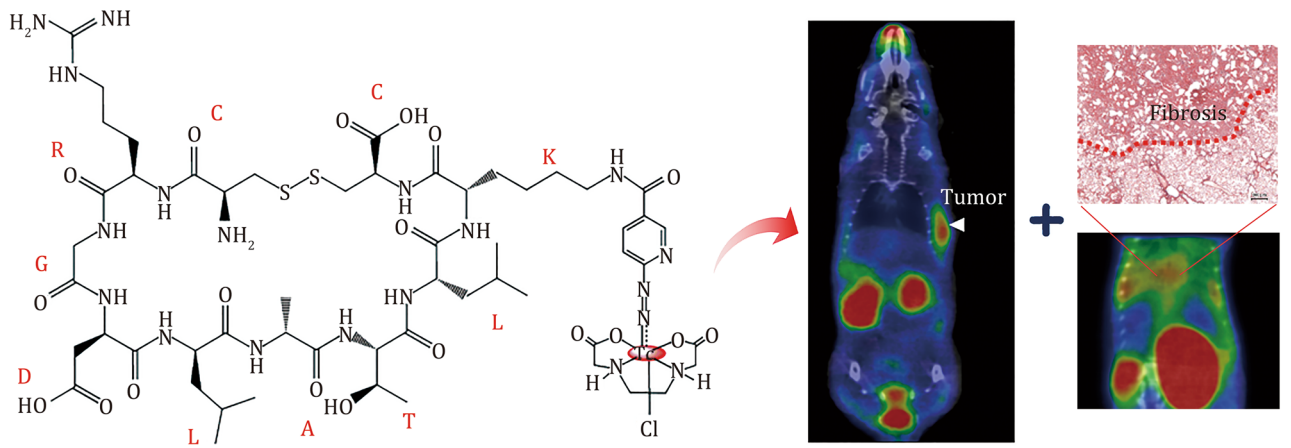

Abstract Integrin αvβ6 is expressed at an undetectable level in normal tissues, but is remarkably upregulated during many pathological processes, especially in cancer and fibrosis. Noninvasive imaging of integrin αvβ6 expression using a radiotracer with favorable *in vivo* pharmacokinetics would facilitate disease diagnosis and therapy monitoring. Through disulfide-cyclized method, we synthesized in this study, a new integrin αvβ6-targeted cyclic peptide (denoted as cHK), and radiolabeled it with ^{99m}Tc. The ability of the resulting radiotracer ^{99m}Tc–HYNIC–cHK to detect integrin αvβ6 expression in pancreatic cancer xenografts and idiopathic pulmonary fibrosis was evaluated using small-animal single-photon emission

✉ Correspondence: liuzf@bjmu.edu.cn (Z. Liu), wangfan@bjmu.edu.cn (F. Wang)

computed tomography (SPECT)/computed tomography (CT). ^{99m}Tc–HYNIC–cHK showed significantly improved *in vivo* metabolic stability compared to the linear peptide-based radiotracer ^{99m}Tc–HYNIC–HK. ^{99m}Tc–HYNIC–cHK exhibited similar biodistribution properties to ^{99m}Tc–HYNIC–HK, but the tumor-to-muscle ratio was significantly increased (2.99 ± 0.87 vs. 1.82 ± 0.27, $P < 0.05$). High-contrast images of integrin αvβ6-positive tumors and bleomycin-induced fibrotic lungs were obtained by SPECT/CT imaging using ^{99m}Tc–HYNIC–cHK. Overall, our studies demonstrate that ^{99m}Tc–HYNIC–cHK is a promising SPECT radiotracer for the noninvasive imaging of integrin αvβ6 in living subjects.

Keywords Integrin αvβ6, Pancreatic cancer, Pulmonary fibrosis, Molecular imaging, Peptide cyclization, Single-photon emission computed tomography (SPECT)

INTRODUCTION

Integrin αvβ6, a member of the integrin family, is present at undetectable levels in adult differentiated tissues, but is overexpressed during embryogenesis, tumorigenesis, and tissue injury (Breuss *et al*. 1993; Desgrosellier and Cheresh 2010; Peng *et al*. 2016). Increased expression of integrin αvβ6 usually correlates with more aggressive disease and poor prognosis (Bates and Mercurio 2005; Elayadi *et al*. 2007; Lee *et al*. 2006), and the upregulation of integrin αvβ6 expression in a wide variety of cancers is associated with increased tumor cells migration, invasion, and metastasis (Bates 2005; Bates and Mercurio 2005). In addition to caner, de novo or increased expression of integrin αvβ6 has also been observed in pathological process of fibrosis (Patsenker *et al*. 2008; Pi *et al*. 2015). Idiopathic pulmonary fibrosis (IPF) is a chronic and progressive fibrotic lung disease with a poor prognosis (Gribbin *et al*. 2006; Navaratnam *et al*. 2011; Wells 2013). Integrin αvβ6-mediated transforming growth factor (TGF)-β activation has been implicated in multiple models of lung fibrosis, and the upregulated expression of integrin αvβ6 has also been found in patients with IPF (Horan *et al*. 2008; Xu *et al*. 2009). Importantly, the expression of integrin αvβ6 is temporally and spatially associated with the course of the fibrosis progression (Puthawala *et al*. 2008).

Due to the critical role of integrin αvβ6 in tumorigenesis and fibrogenesis, it has emerged as an appealing target for diagnostic imaging, prognosis evaluation, and therapeutic responses monitoring (Agarwal 2014; Cantor *et al*. 2015; Saini *et al*. 2015; Yang *et al*. 2015). Therefore, noninvasive and quantitative imaging of integrin αvβ6 expression by molecular imaging techniques would be of great potential for better management of these diseases. Previous studies have focused on the development of positron emission tomography (PET) and single-photon emission computed tomography (SPECT) radiotracers for *in vivo* imaging of integrin αvβ6 expression (Hackel *et al*. 2013; Hausner *et al*. 2007, 2008, 2009a, b, 2013; Hu *et al*. 2014; John *et al*. 2013; Kimura *et al*. 2012; Li *et al*. 2011; Liu *et al*. 2014b; Man *et al*. 2013; Nothelfer *et al*. 2009; Saha *et al*. 2010; Satpati *et al*. 2014; Singh *et al*. 2014; Ueda *et al*. 2014; Zhu *et al*. 2014). Although promising, most of these radiotracers are based on linear peptides, which have poor *in vivo* metabolic stability and suboptimal pharmacokinetics. For example, we observed recently that a ^{99m}Tc-labeled linear peptide (RGDLATLRQLAQEDGVVGVRK, the HK peptide) completely degraded *in vivo* within 30 min after injection, leading to a very low tumor uptake and tumor-to-nontumor ratios (Liu *et al*. 2014b).

Peptide cyclization has been reported to be a powerful strategy to improve the stability of peptides by means of adopted resistance to enzymatic degradation (Besser *et al*. 2000; Bogdanowich-Knipp *et al*. 1999a, b; Gilon *et al*. 1991; Pakkala *et al*. 2007; Roxin and Zheng 2012; Shi *et al*. 2016). To overcome the limitations of ^{99m}Tc-labeled HK peptide, in this study, we selected the first seven amino acid residues of the integrin αvβ6-targeting HK peptide and added a lysine residue at C-terminal in order to conjugate the chelator. We then cyclized it by adding a cysteine residue at N- and C-terminals, respectively, to generate a new peptide c (CRGDLATLKC, denoted as cHK). The peptide cHK was conjugated with the chelator sodium succinimidyl 6-(2-(2-sulfonatobenzaldehyde) hydrazono) nicotinate (HYNIC)-NHS and then radiolabeled with ^{99m}Tc. The resulting radiotracer ^{99m}Tc–HYNIC–cHK was evaluated *in vivo* as a SPECT radiotracer for imaging of integrin αvβ6 expression in both cancer and IPF mouse models.

RESULTS

Chemistry and radiochemistry

The Fmoc-cHK–HYNIC conjugate (Fig. 1A) was prepared by direct conjugation of Fmoc-cHK peptide with

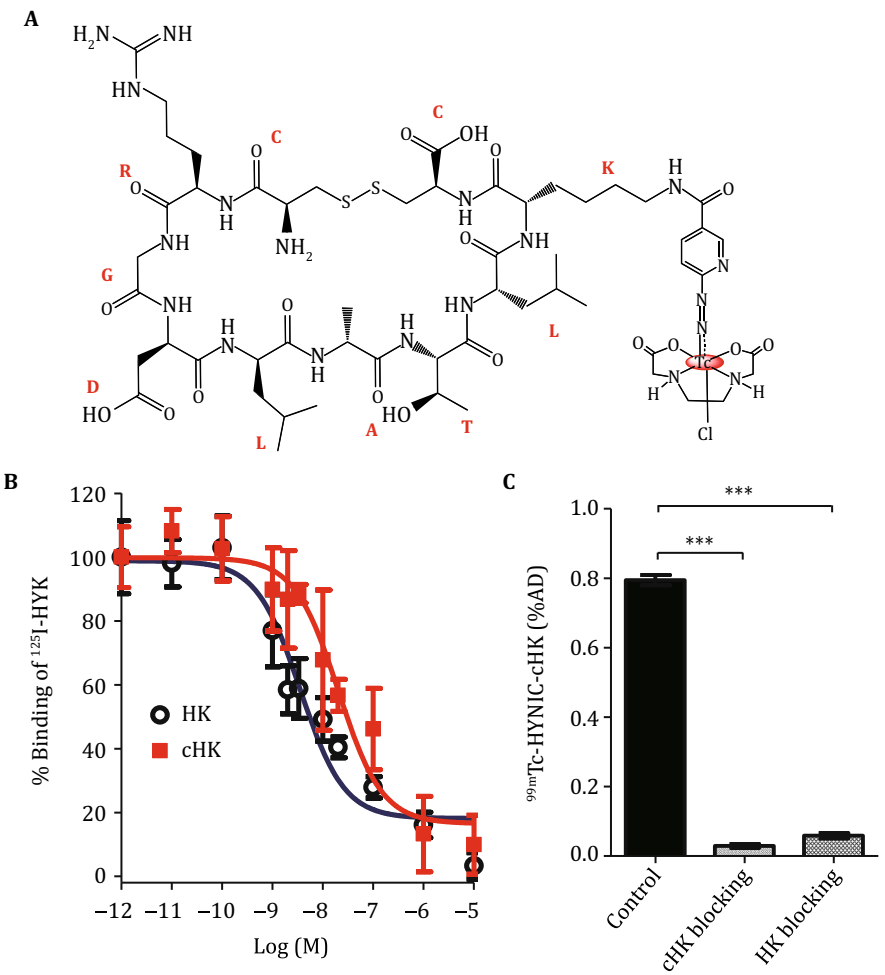

Fig. 1 **A** Chemical structure of ^{99m}Tc–HYNIC–cHK. **B** Inhibition of ^{125}I–HYK binding to integrin αvβ6 on BxPC-3 cells by the cHK and HK peptides. **C** Binding of ^{99m}Tc–HYNIC–cHK to BxPC-3 cells (without or with 300 μg of HK/cHK peptide blocking), $^{***}P < 0.001$

HYNIC-NHS. After the removal of Fmoc group, the final product HYNIC–cHK was confirmed by high-performance liquid chromatography (HPLC) and mass spectrometry. The HPLC purity of HYNIC–cHK was >95% before being used for ^{99m}Tc radiolabeling. The ^{99m}Tc-labeling procedure was done within 30 min with a yield ranging from 85% to 90%. The radiochemical purity was >95% after purification, and the specific activity was >30 MBq/nmol.

Cell-binding assay

Similar to the HK peptide, cHK peptide also inhibited the binding of ^{125}I–RGDLATLRQLAQEDGVVGVRYK (HYK) to integrin αvβ6-expressing BxPC-3 cells in a concentration-dependent manner, but the integrin αvβ6 binding affinity of cHK was lower compared to that of HK peptide. The IC_{50} values for cHK and HK were 20.25 ± 1.17 and 3.55 ± 0.09 nmol/L, respectively (Fig. 1B).

The binding specificity of ^{99m}Tc–HYNIC–cHK to integrin αvβ6 was evaluated in integrin αvβ6-positive BxPC-3 cells. As shown in Fig. 1C, the binding of ^{99m}Tc–HYNIC–cHK to BxPC-3 cells was significantly inhibited by the addition of excess doses of the cHK and HK peptides (from 0.79 ± 0.01 %AD to 0.03 ± 0.005 and 0.06 ± 0.007 %AD, respectively, $P < 0.001$).

Solution and metabolic stability

The *in vitro* solution stability of ^{99m}Tc–HYNIC–cHK in fetal bovine serum (FBS) or L-cysteine was monitored by radio-HPLC. Figure 2A shows that ^{99m}Tc–HYNIC–cHK remains stable for more than 4 h both in FBS and in the presence of L-cysteine.

We performed the metabolism studies of ^{99m}Tc–HYNIC–cHK using normal BALB/c mice. We analyzed the samples from both blood and urine to determine whether the radiotracer retains its chemical integrity at 0.5 h and 1 h postinjection. Figures 2B–F illustrate the radio-HPLC chromatograms of ^{99m}Tc–HYNIC–cHK before injection (Fig. 2B), in the blood (Fig. 2C, E) and in the urine (Fig. 2D, F). ^{99m}Tc–HYNIC–cHK retained its integrity in urine, while showing the degrees of metabolism to be 9.94% and

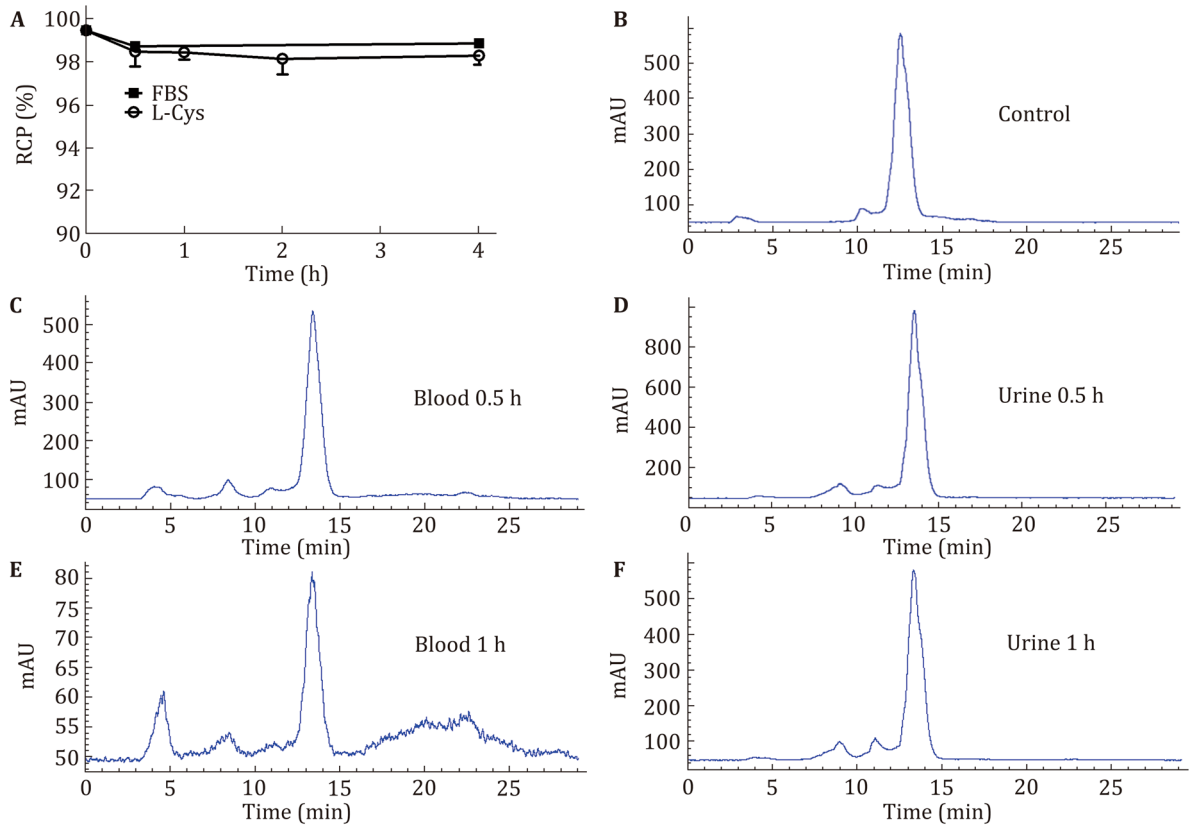

Fig. 2 **A** Solution stability of ^{99m}Tc–HYNIC–cHK in serum and L-cysteine (1.0 mg/mL). **B–F** Typical radio-HPLC chromatogram and metabolic stability of ^{99m}Tc–HYNIC–cHK in mouse blood and urine at 0.5 and 1 h after injection

30.09% in blood at 0.5 h and 1 h postinjection, respectively. Compared to the linear peptide-based radiotracer ^{99m}Tc–HYNIC–HK (Liu *et al.* 2014b), ^{99m}Tc–HYNIC–cHK is much more stable *in vivo*.

Biodistribution

As shown in Fig. 3A, the uptake values of ^{99m}Tc–HYNIC–cHK in BxPC-3 tumors were 0.63 ± 0.18, 0.43 ± 0.09, and 0.33 ± 0.16 %ID/g at 0.5, 1, and 2 h after injection, respectively. The tumor uptake of ^{99m}Tc–HYNIC–cHK was higher than that in most of the normal organs, such as heart, liver, pancreas, bone, and muscle, at almost all time points examined ($P < 0.05$). The tumor uptake of ^{99m}Tc–HYNIC–cHK was significantly reduced with a coinjection of an excess dose of the cold HK peptide at 1 h after injection (from 0.43 ± 0.09 to 0.24 ± 0.04 %ID/g, $n = 4$, $P < 0.01$).

The uptake of ^{99m}Tc–HYNIC–cHK was similar to ^{99m}Tc–HYNIC–HK in BxPC-3 tumors at 0.5 h after injection (0.63 ± 0.18 vs. 0.58 ± 0.09, $n = 4$, $P > 0.05$). However, the uptake of ^{99m}Tc–HYNIC–cHK in muscle or bone was much lower, and the tumor-to-muscle (T/M) ratio was significantly higher than that of ^{99m}Tc–HHK (2.99 ± 0.87 vs. 1.82 ± 0.27, $n = 4$, $P < 0.05$; Fig. 3B).

SPECT imaging of BxPC-3 cancer xenografts

Representative small-animal SPECT/CT images of BxPC-3 tumor-bearing mice at 0.5 h and 1 h after intravenous injection of ^{99m}Tc–HYNIC–cHK are shown in Fig. 4A. The radiotracer showed clear tumor imaging with high contrast to the contralateral background. The *in vivo* receptor-binding property of ^{99m}Tc–HYNIC–cHK was determined by the blocking study. The tumor uptake of ^{99m}Tc–HYNIC–cHK was almost completely inhibited in the HK blocking group ($P < 0.001$; Fig. 4B, C).

SPECT/CT imaging of bleomycin-induced pulmonary fibrosis

As shown in Fig. 5A, markedly gray regions were observed by CT imaging in the lung areas of mice in the bleomycin (BLM)-treated mice, suggesting the evident fibrosis formation induced by BLM. Notably, an evident accumulation of ^{99m}Tc–HYNIC–cHK in the lungs of the BLM-treated mice was observed. In contrast, no

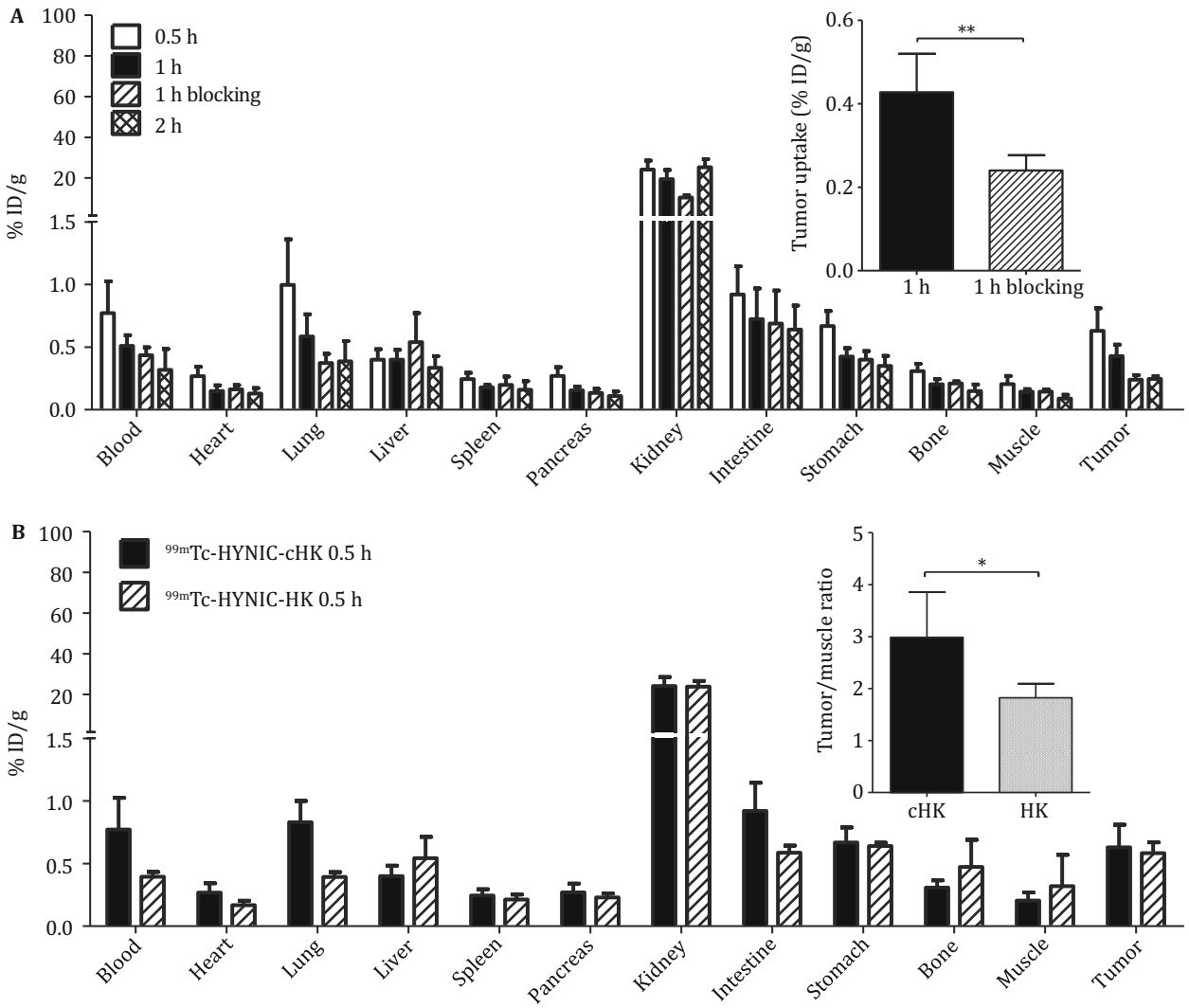

Fig. 3 **A** Biodistribution of ^{99m}Tc–HYNIC–cHK in BxPC-3 tumor-bearing nude mice at 0.5, 1, and 2 h after injection and coinjected with cold HK peptide at 1 h after injection. Inset: enlarged view of the tumor uptake values; $^{**}P < 0.01$. **B** Biodistribution of ^{99m}Tc–HYNIC–cHK and ^{99m}Tc–HHK in BxPC-3 tumor-bearing nude mice at 0.5 h after injection. Inset: enlarged view of the tumor-to-muscle ratios; $^{*}P < 0.05$

significant uptake of ^{99m}Tc–HYNIC–cHK was observed in the phosphate-buffered saline (PBS)-treated mice (Fig. 5A, B). After the SPECT/CT imaging, the mice were sacrificed, and the presence of fibrosis in the edge of pulmonary lobes were verified by anatomic visualization after dissection in the BLM group. The hematoxylin–eosin (H&E) and Sirius red (specific for collagen) staining further confirmed the SPECT/CT findings (Fig. 5C).

DISCUSSION

Overexpression of integrin αvβ6 has been found in approximately 100% of pancreatic cancers (Liu *et al.* 2014a). Integrin αvβ6-targeted imaging for pancreatic cancer detection and staging would contribute to improve the prospect of curing or controlling pancreatic cancer. We previously synthesized a linear peptide-based SPECT radiotracer (^{99m}Tc–HYNIC–HK) and demonstrated its potential for the specific detection of subcutaneous pancreatic tumor xenografts and liver metastases in mouse models (Liu *et al.* 2014b). However, ^{99m}Tc–HYNIC–HK had a very poor *in vivo* stability, which may significantly hamper its potential clinical translation. There are several approaches to improve the *in vivo* stability of peptides, including changing some amino acids of the peptide into D-amino acids, cyclizing the peptide to be a cyclic peptide, or engineering the peptide into scaffold-based peptides, such as cysteine knot (Zhu *et al.* 2014). In this study, we synthesized a cyclic peptide based on the HK peptide, and

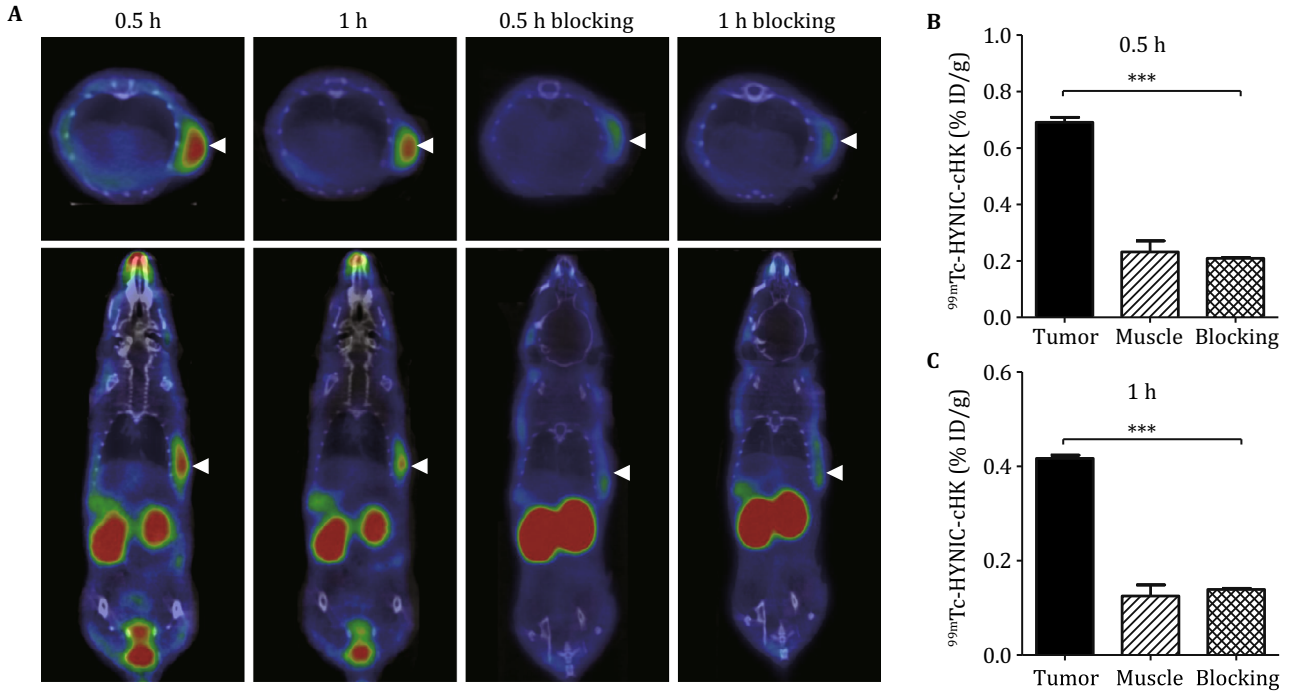

Fig. 4 **A** Representative small-animal SPECT/CT images obtained at 0.5 and 1 h after injection of ^{99m}Tc–HYNIC–cHK nude mice in BxPC-3 tumor-bearing nude mice without or with blocking dose of cold HK peptide. Arrows indicate the location of tumors. **B–C** Quantitation of tumor and muscle uptakes of ^{99m}Tc–HYNIC–cHK from SPECT scanning, $^{***}P < 0.001$

radiolabeled it with ^{99m}Tc, the resulting radiotracer ^{99m}Tc–HYNIC–cHK was evaluated both *in vitro* and *in vivo*.

Through the *in vitro* solution stability study, ^{99m}Tc–HYNIC–cHK was demonstrated to be rather stable in FBS or L-cysteine over 4 h. The *in vivo* metabolic study indicated that the stability in blood was considerably improved after cyclization (Fig. 2). Afterward, the integrin αvβ6-targeting ability of ^{99m}Tc–HYNIC–cHK was evaluated through cell-binding assays in integrin αvβ6-positive BxPC-3 cells. Similar to the HK peptide, cHK could also inhibit the binding of ^{125}I–HYK on BxPC-3 cells in a dose-dependent manner. However, the binding affinity of cHK to integrin αvβ6 was slightly lower than that of the HK peptide. The decreased affinity may result from the shortened peptide sequence and constrained conformation of the cyclic peptide compared to the linear peptide. ^{99m}Tc–HYNIC–cHK retains the integrin αvβ6-targeting capability as evidenced by the significantly inhibited binding by adding an excess of cold cHK or HK peptide (Fig. 1C).

The *in vivo* integrin αvβ6-targeting specificity of ^{99m}Tc–HYNIC–cHK was confirmed by the biodistribution and SPECT/CT imaging studies in the BxPC-3 xenograft tumors. ^{99m}Tc–HYNIC–cHK exhibited rapid tumor accumulation and showed the maximum tumor-uptake values at 0.5 h after injection (Fig. 3A). Predominant kidney uptake of ^{99m}Tc–HYNIC–cHK was also observed, most likely due to the renal clearance of this radiotracer. The absolute tumor uptake of ^{99m}Tc–HYNIC–cHK was comparable to that of ^{99m}Tc–HHK at 0.5 h (Fig. 3). However, the tumor-to-muscle ratio was significantly higher for ^{99m}Tc–HYNIC–cHK compared to that of ^{99m}Tc-HHK, resulting in a favorable tumor imaging contrast.

In addition to cancer, *de novo* and increased expression of integrin αvβ6 also occur during fibrogenesis. The increased expression of integrin αvβ6 has been found in fibrotic lung tissue in patients with IPF and was demonstrated to play an important role in the progression of lung fibrotic disease in several different studies (Horan *et al*. 2008; Puthawala *et al*. 2008; Xu *et al*. 2009). To date, the only approach to detect the expression of integrin αvβ6 in the fibrotic lung is immunohistochemical analysis of biopsy samples (Raghu *et al*. 2011). This procedure is clinically impractical for many patients and suffers from sampling bias, resulting in incomplete information. Considering the high short-term mortality following lung biopsy (Utz *et al*. 2001), repeated sampling is unrealistic. Hence, noninvasive molecular imaging of integrin αvβ6 expression would offer a remarkable improvement for immunophenotyping patients with IPF. ^{18}F–FDG and ^{68}Ga-labeled somatostatin analogs targeting somatostatin receptor as PET tracers have been used for IPF

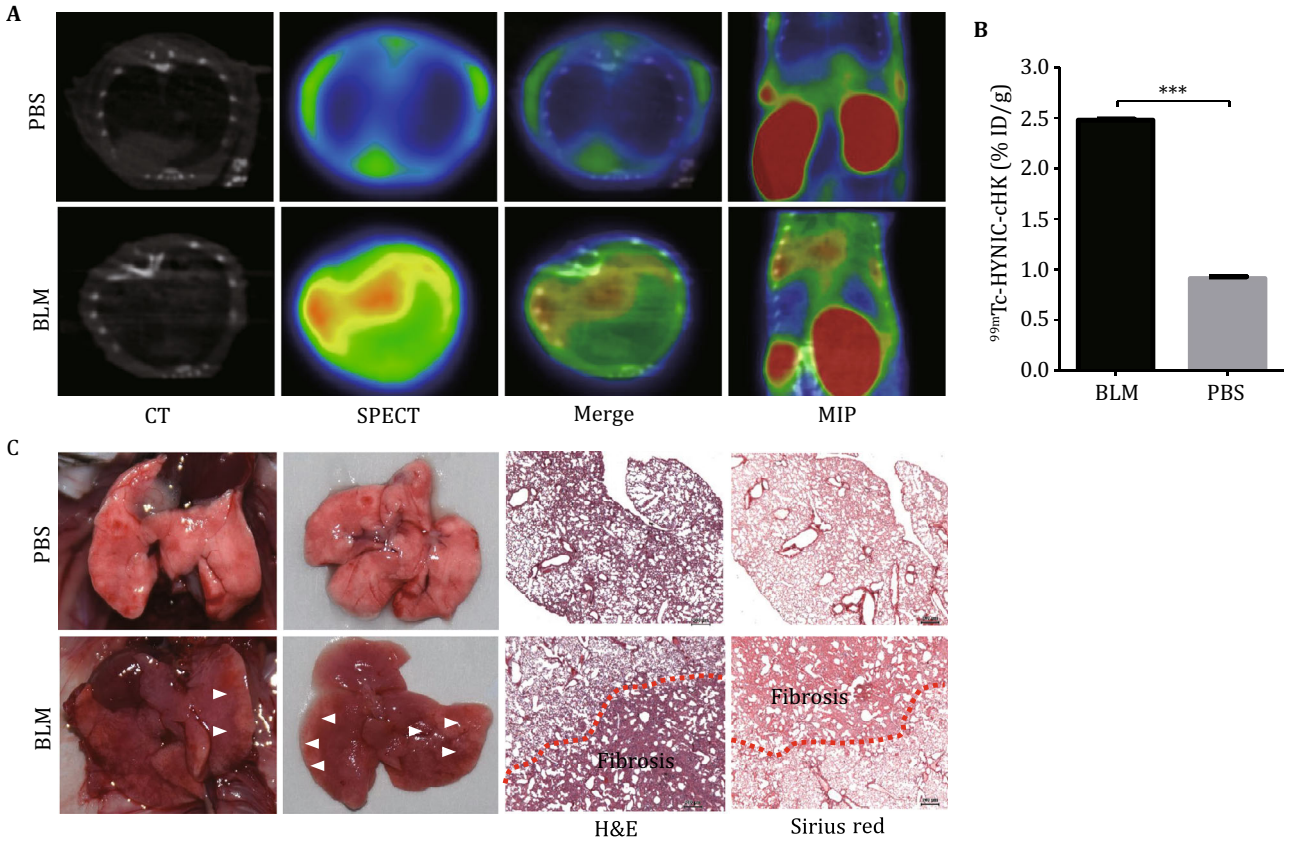

Fig. 5 **A** Representative SPECT/CT images of ^{99m}Tc–HYNIC–cHK in BLM-treated and PBS-treated C57/BL6 mice at 0.5 h after injection. **B** Quantitation of lung uptakes of ^{99m}Tc–HYNIC–cHK in BLM-treated and PBS-treated C57/BL6 mice from the SPECT scanning, $^{***}P < 0.001$. **C** Gross observation of the lungs, and H&E and Sirius red staining of the lung tissues from BLM-treated and PBS-treated C57/BL6 mice

stratification, but neither of these radiotracers targets well-validated pathways implicated in IPF (Ambrosini *et al*. 2010; Win *et al*. 2012). Cai *et al*. recently developed an optical activatable probe for noninvasive diagnosis of IPF by targeting matrix metalloproteinase type 2 (MMP-2), which was also correlated with IPF development. However, MMP-2 could be secreted into the blood stream, the nonspecific fluorescence signal recovery in tissues (*e.g.* liver) other than lung was noticed over time (Cai *et al*. 2013). John *et al*. developed an ^{111}In-labeled αvβ6-specific peptide (^{111}In–DTPA–A20FMDV2) as a SPECT radiotracer and for the first time used it for noninvasive measurement of integrin αvβ6 expression in lungs of mice with BLM-induced fibrosis (John *et al*. 2013). Their results showed that the lung uptake of ^{111}In–DTPA–A20FMDV2 is quantifiable and correlates with the levels of αvβ6 protein, itgb6 messenger RNA, and hydroxyproline in the lungs.

The low uptake of ^{99m}Tc–HYNIC–cHK in normal lungs makes it a potential tool for quantitative and global analyses of integrin αvβ6 expression with high sensitivity in imaging the lung disorders. In the murine model of pulmonary fibrosis induced by BLM, a significant accumulating of ^{99m}Tc–HYNIC–cHK in lungs of BLM-treated mice was observed, compared with the PBS group (Fig. 5A, B). The H&E and Sirius red staining confirmed the lung fibrotic lesions in the lungs of BLM-treated mice (Fig. 5C). Compared with ^{111}In, ^{99m}Tc is more suitable for labeling peptide-based probes because that the radioactive half-life of ^{99m}Tc matches the metabolic half-life of peptides. Moreover, ^{99m}Tc-labeled radiotracer is more widely available and cost effective. The high labeling yield of ^{99m}Tc chelator systems also allows the formulation of kits for the rapid preparation of radiotracers for widespread applications.

Although the metabolic stability of ^{99m}Tc–HYNIC–cHK after cyclization was significant improved compared to the linear radiotracer ^{99m}Tc–HYNIC–HK, the receptor-binding affinity of ^{99m}Tc–HYNIC–cHK was slightly decreased. In order to increase the receptor-binding affinity and further improve the *in vivo* pharmacokinetics of ^{99m}Tc–HYNIC–cHK, efforts such as polyethylene glycol (PEG)ylation and multimerization may be required to further optimize this radiotracer.

CONCLUSION

A cyclic peptide-based radiotracer ^{99m}Tc–HYNIC–cHK with improved *in vivo* metabolic stability was prepared and evaluated both *in vitro* and *in vivo*. ^{99m}Tc–HYNIC–cHK exhibited specific integrin αvβ6-targeting ability and was demonstrated to specific detection of integrin αvβ6 expression in subcutaneous pancreatic cancer xenografts and pulmonary fibrosis in animal models. Further optimization of ^{99m}Tc–HYNIC–cHK may eventually yield a clinical applicable radiotracer for SPECT imaging of integrin αvβ6 expression, disease staging, and monitoring of therapy efficacy.

EXPERIMENTAL SECTION

Materials and reagents

All commercially available chemical reagents were used without further purification unless otherwise stated. The peptides Fmoc-cHK, HYK and HK were synthesized by ChinaPeptide Co., Ltd (Shanghai, China). $Na^{99m}TcO_4$ was obtained from a commercial ^{99}Mo/^{99m}Tc generator (Beijing Atom High Tech Co., Beijing, China). The reversed-phase high-performance liquid chromatography (HPLC) system was Agilent Technologies 1260 Infinity HPLC (Agilent Technologies, Santa Clara, CA) coupled with the Raytest Gabi radioactivity detector (Raytest, Straubenhardt, Germany). Female BALB/c nude mice (4–5 weeks of age), BALB/c normal mice (4–5 weeks of age), and C57/BL6 mice (7–8 weeks of age) were purchased from Department of Laboratory Animal Science, Peking University Health Science Center (Beijing, China). BLM was purchased from Aladdin (Shanghai, China).

Synthesis of HYNIC-conjugated cHK peptide

The Fmoc-cHK peptide was conjugated with HYNIC–NHS using a standard procedure. Briefly, a solution of Fmoc-cHK was mixed with HYNIC–NHS at a mole ratio of 1:1.2. The pH was adjusted to 8.5–9.0 using *N*,*N*-Diisopropylethylamine. After stirring for 4 h at room temperature, the Fomc was removed by adding piperidine with a final volume fraction of 20%. The HYNIC–cHK was isolated by semi-preparative HPLC and lyophilized to afford the final product as a white powder (yield: 56%). Analytical HPLC (Retention time = 14.99 min) and mass spectrometry (MALDI-TOF–MS: *m*/*z*, 1380.66 for $[MH]^+$ ($C_{56}H_{85}N_{17}O_{18}S_3$, calculated molecular weight 1380.57) confirmed the identity of the product.

Preparation of ^{99m}Tc–HYNIC–cHK

For ^{99m}Tc labeling, a mixture of 20 mg tricine (100 mg/mL in 25 mmol/L succinate buffer, pH 5.0), 740 MBq (20 mCi) $Na^{99m}TcO_4$, and 30 μl $SnCl_2$ (1 μg/μL in 0.1 mol/L HCl) was successively added to 20 μg of HYNIC–cHK with constant stirring at 99 °C for 10 min. Then 100 μl of ethylenediamine-*N*,*N*′-diacetic acid (100 mg/mL) was added to the mixture with contant stirring at 99 °C for 20 min. After allowing it to cool down to room temperature, the mixture was purified with Sep-Pak C18 cartridges (Waters) as preciously described (Jia *et al*. 2006).

Cell culture and animal models

The BxPC-3 human pancreatic cancer cell line was obtained from American Type Culture Collection. Cells were cultured in RPMI-1640 medium supplemented with 10% FBS at 37 °C in humidified atmosphere containing 5% CO_2.

All animal experiments were performed in accordance with the guidelines of Peking University Animal Care and Use Committee. To establish the BxPC-3 subcutaneous tumor model, BxPC-3 cells (1×10^7 in 100 μl of PBS) were inoculated subcutaneously into the right front flanks of female BALB/c nude mice. The animals were used for *in vivo* studies when the tumor size reached 200–300 mm^3 (3–4 weeks after inoculation). For the pulmonary fibrosis mouse model, BLM (1.5 units/kg, 50 μl in PBS) or PBS (50 μl; as a vehicle control) was administered once into the C57/BL6 mice by intratracheal injection. On day 21 (based on pilot studies), the mice with well-established pulmonary fibrosis were used for SPECT/CT imaging.

Integrin αvβ6 binding specificity

In vitro integrin αvβ6 binding affinities of cHK and HK were compared via displacement cell-binding assays (Dong *et al*. 2015) using ^{125}I–HYK as the radioligand. ^{125}I–HYK was prepared by labeling HYK with $Na^{125}I$ using the Iodogen method as previously reported (Liu *et al*. 2010). Experiments were performed on high integrin αvβ6-expressing BxPC-3 cells. The best-fit 50% inhibitory concentration (IC_{50}) values were calculated by fitting the data with nonlinear regression using Graph-Pad Prism (GraphPad Software, Inc.).

In vitro integrin αvβ6 binding specificity of ^{99m}Tc–HYNIC–cHK was tested using the integrin αvβ6-positive BxPC-3 cells. Briefly, cells were seeded into 12-well plates and incubated overnight at 37 °C to allow adherence. After brief washing with PBS, tumor cells

were incubated with 3.7 kBq ^{99m}Tc–HYNIC–cHK with or without an excess dose of cold cHK or HK peptide at 4 °C for 4 h. Tumor cells were then washed with chilled PBS and harvested by trypsinization with 0.05% trypsin. The cell suspensions were collected and measured in a γ-counter (Wallac 1470-002, Perkin-Elmer, Finland). The cell uptake was expressed as the percent added dose (%AD). Experiments were performed twice with triplicate samples.

Solution and metabolic stability

^{99m}Tc–HYNIC–cHK was incubated in FBS or L-cysteine (1.0 mg/mL) for 0, 0.5, 1, 2, and 4 h at 37 °C to test the *in vitro* solution stability. After passing through a 0.22-μm Millipore filter, the samples were analyzed by radio-HPLC.

The metabolic stability of ^{99m}Tc–HYNIC–cHK was evaluated in female BALB/c normal mice. Each mouse was administered with the radiotracer at a dose of 1 mCi in 100 μl saline via intravenous injection. At 0.5 h and 1 h postinjection, the blood and urine samples were collected. The samples were centrifuged at 8000 r/min for 15 min. The supernatant was collected, filtered through a 0.22-μm Millipore filter, and then analyzed by radio-HPLC.

Biodistribution

Biodistribution studies were performed using female BALB/c nude mice bearing BxPC-3 xenografts. Mice received an injection via the tail vein of 370 kBq (10 μCi) of ^{99m}Tc–HYNIC–cHK to evaluate the distribution of the radiotracer. The blocking experiments were also performed by coinjection of ^{99m}Tc–HYNIC–cHK with a saturating dose of the HK peptide (500 μg per mouse). At 0.5, 1, and 2 h after injection, the animals were sacrificed, and the tumors and the organs/tissues of interest were dissected and wet-weighed, and the radioactivity in the tissue was measured using a γ-counter. The results are presented as percentages of injected dose per gram of tissue (%ID/g). Values are expressed as mean ± SD (n = 4 per group).

Small-animal SPECT/CT imaging

Small-animal SPECT/CT scans of subcutaneous BxPC-3 tumor and pulmonary fibrosis mouse models were performed using a SPECT/CT system (NanoScan; Mediso, Budapest, Hungary). Each BxPC-3-bearing mouse was injected via tail vein with 37 MBq (1 mCi) of ^{99m}Tc–HYNIC–cHK. At 0.5 h and 1 h after injection, the mice were anesthetized by inhalation of 2% isoflurane and imaged using the Nano-SPECT/CT camera, The SPECT and CT fusion images were obtained using the automatic fusion software (InterView Fusion; Mediso Medical Imaging Systems, Budapest, Hungary).

Each BLM- or PBS-treated mouse was administered with 37 MBq of ^{99m}Tc–HYNIC–cHK via tail vein. After SPECT/CT imaging, the BLM- and PBS-treated mice were euthanized. Lungs were excised and fixed in 5% buffered formalin, embedded in paraffin, and cut into sections for staining with H&E or Sirius red as previously described (Yu *et al*. 2016).

Statistical analysis

Quantitative data were expressed as mean ± SD. Results were compared using the Student t test. P values of less than 0.05 were considered statistically significant.

Acknowledgments This work was partially supported by the National Key R&D Program of China (2018YFC1313300 and 2017YFA0205600), the National Natural Science Foundation of China (81471712, 81671747, 81630045, 81873907, and 81420108019), the Beijing Natural Science Foundation (L172007), the Beijing Nova Program Interdisciplinary Cooperation Project (Z181100006218136), and the Clinical Medicine Plus X-Young Scholars Project of Peking University (PKU2018LCXQ017).

Compliance with ethics standards

Conflict of interest Hao Liu, Liquan Gao, Xinhe Yu, Lijun Zhong, Jiyun Shi, Bing Jia, Nan Li, Zhaofei Liu, and Fan Wang declare that they have no conflicts of interest.

Human and animal rights and informed consent All institutional and national guidelines for the care and use of laboratory animals were followed. This article does not contain any studies with human subjects performed by any of the authors.

References

Agarwal SK (2014) Integrins and cadherins as therapeutic targets in fibrosis. Front Pharmacol 5:131

Ambrosini V, Zompatori M, De Luca F, Antonia D, Allegri V, Nanni C, Malvi D, Tonveronachi E, Fasano L, Fabbri M, Fanti S (2010) ^{68}Ga-DOTANOC PET/CT allows somatostatin receptor imaging in idiopathic pulmonary fibrosis: preliminary results. J Nucl Med 51:1950–1955

Bates RC (2005) Colorectal cancer progression: integrin alphavbeta6 and the epithelial-mesenchymal transition (EMT). Cell Cycle 4:1350–1352

Bates RC, Mercurio AM (2005) The epithelial-mesenchymal transition (EMT) and colorectal cancer progression. Cancer Biol Ther 4:365–370

Besser D, Muller B, Kleinwachter P, Greiner G, Seyfarth L, Steinmetzer T, Arad O, Reissmann S (2000) Synthesis and characterization of octapeptide somatostatin analogues with backbone cyclization: comparison of different strategies, biological activities and enzymatic stabilities. J Prakt Chem 342:537–545

Bogdanowich-Knipp SJ, Chakrabarti S, Williams TD, Dillman RK, Siahaan TJ (1999a) Solution stability of linear vs. cyclic RGD peptides. J Pept Res 53:530–541

Bogdanowich-Knipp SJ, Jois DS, Siahaan TJ (1999b) The effect of conformation on the solution stability of linear vs. cyclic RGD peptides. J Pept Res 53:523–529

Breuss JM, Gillett N, Lu L, Sheppard D, Pytela R (1993) Restricted distribution of integrin beta6 mRNA in primate epithelial tissues. J Histochem Cytochem 41:1521–1527

Cai Y, Zhu L, Zhang F, Niu G, Lee S, Kimura S, Chen X (2013) Noninvasive monitoring of pulmonary fibrosis by targeting matrix metalloproteinases (MMPs). Mol Pharm 10:2237–2247

Cantor DI, Cheruku HR, Nice EC, Baker MS (2015) Integrin alphavbeta6 sets the stage for colorectal cancer metastasis. Cancer Metastasis Rev 34:715–734

Desgrosellier JS, Cheresh DA (2010) Integrins in cancer: biological implications and therapeutic opportunities. Nat Rev Cancer 10:9–22

Dong C, Liu Z, Wang F (2015) Radioligand saturation binding for quantitative analysis of ligand-receptor interactions. Biophys Rep 1:148–155

Elayadi AN, Samli KN, Prudkin L, Liu YH, Bian A, Xie XJ, Wistuba II, Roth JA, McGuire MJ, Brown KC (2007) A peptide selected by biopanning identifies the integrin alphavbeta6 as a prognostic biomarker for nonsmall cell lung cancer. Cancer Res 67:5889–5895

Gilon C, Halle D, Chorev M, Selinger Z, Byk G (1991) Backbone cyclization: a new method for conferring conformational constraint on peptides. Biopolymers 31:745–750

Gribbin J, Hubbard RB, Le Jeune I, Smith CJ, West J, Tata LJ (2006) Incidence and mortality of idiopathic pulmonary fibrosis and sarcoidosis in the UK. Thorax 61:980–985

Hackel BJ, Kimura RH, Miao Z, Liu H, Sathirachinda A, Cheng Z, Chin FT, Gambhir SS (2013) ^{18}F-fluorobenzoate-labeled cystine knot peptides for PET imaging of integrin alphavbeta6. J Nucl Med 54:1101–1105

Hausner SH, DiCara D, Marik J, Marshall JF, Sutcliffe JL (2007) Use of a peptide derived from foot-and-mouth disease virus for the noninvasive imaging of human cancer: generation and evaluation of 4-[^{18}F]fluorobenzoyl A20FMDV2 for *in vivo* imaging of integrin alphavbeta6 expression with positron emission tomography. Cancer Res 67:7833–7840

Hausner SH, Marik J, Gagnon MK, Sutcliffe JL (2008) *In vivo* positron emission tomography (PET) imaging with an alphavbeta6 specific peptide radiolabeled using ^{18}F-"click" chemistry: evaluation and comparison with the corresponding 4-[^{18}F]fluorobenzoyl- and 2-[^{18}F]fluoropropionyl-peptides. J Med Chem 51:5901–5904

Hausner SH, Abbey CK, Bold RJ, Gagnon MK, Marik J, Marshall JF, Stanecki CE, Sutcliffe JL (2009a) Targeted *in vivo* imaging of integrin alphavbeta6 with an improved radiotracer and its relevance in a pancreatic tumor model. Cancer Res 69:5843–5850

Hausner SH, Kukis DL, Gagnon MK, Stanecki CE, Ferdani R, Marshall JF, Anderson CJ, Sutcliffe JL (2009b) Evaluation of [^{64}Cu]Cu-DOTA and [^{64}Cu]Cu-CB-TE2A chelates for targeted positron emission tomography with an alphavbeta6-specific peptide. Mol Imaging 8:111–121

Hausner SH, Carpenter RD, Bauer N, Sutcliffe JL (2013) Evaluation of an integrin alphavbeta6-specific peptide labeled with [^{18}F]fluorine by copper-free, strain-promoted click chemistry. Nucl Med Biol 40:233–239

Horan GS, Wood S, Ona V, Li DJ, Lukashev ME, Weinreb PH, Simon KJ, Hahm K, Allaire NE, Rinaldi NJ, Goyal J, Feghali-Bostwick CA, Matteson EL, O'Hara C, Lafyatis R, Davis GS, Huang X, Sheppard D, Violette SM (2008) Partial inhibition of integrin alphavbeta6 prevents pulmonary fibrosis without exacerbating inflammation. Am J Respir Crit Care Med 177:56–65

Hu LY, Bauer N, Knight LM, Li Z, Liu S, Anderson CJ, Conti PS, Sutcliffe JL (2014) Characterization and evaluation of ^{64}Cu-labeled A20FMDV2 conjugates for imaging the integrin alphavbeta 6. Mol Imaging Biol 16:567–577

Jia B, Shi J, Yang Z, Xu B, Liu Z, Zhao H, Liu S, Wang F (2006) ^{99m}Tc-labeled cyclic RGDfK dimer: initial evaluation for SPECT imaging of glioma integrin alphavbeta3 expression. Bioconjug Chem 17:1069–1076

John AE, Luckett JC, Tatler AL, Awais RO, Desai A, Habgood A, Ludbrook S, Blanchard AD, Perkins AC, Jenkins RG, Marshall JF (2013) Preclinical SPECT/CT imaging of alphavbeta6 integrins for molecular stratification of idiopathic pulmonary fibrosis. J Nucl Med 54:2146–2152

Kimura RH, Teed R, Hackel BJ, Pysz MA, Chuang CZ, Sathirachinda A, Willmann JK, Gambhir SS (2012) Pharmacokinetically stabilized cystine knot peptides that bind alphavbeta6 integrin with single-digit nanomolar affinities for detection of pancreatic cancer. Clin Cancer Res 18:839–849

Lee JS, Heo J, Libbrecht L, Chu IS, Kaposi-Novak P, Calvisi DF, Mikaelyan A, Roberts LR, Demetris AJ, Sun Z, Nevens F, Roskams T, Thorgeirsson SS (2006) A novel prognostic subtype of human hepatocellular carcinoma derived from hepatic progenitor cells. Nat Med 12:410–416

Li F, Song Z, Li Q, Wu J, Wang J, Xie C, Tu C, Wang J, Huang X, Lu W (2011) Molecular imaging of hepatic stellate cell activity by visualization of hepatic integrin alphavbeta3 expression with SPECT in rat. Hepatology 54:1020–1030

Liu Z, Jin C, Yu Z, Zhang J, Liu Y, Zhao H, Jia B, Wang F (2010) Radioimmunotherapy of human colon cancer xenografts with ^{131}I-labeled anti-CEA monoclonal antibody. Bioconjug Chem 21:314–318

Liu H, Wu Y, Wang F, Liu Z (2014a) Molecular imaging of integrin alphavbeta6 expression in living subjects. Am J Nucl Med Mol Imaging 4:333–345

Liu Z, Liu H, Ma T, Sun X, Shi J, Jia B, Sun Y, Zhan J, Zhang H, Zhu Z, Wang F (2014b) Integrin alphavbeta6-targeted SPECT imaging for pancreatic cancer detection. J Nucl Med 55:989–994

Man YK, DiCara D, Chan N, Vessillier S, Mather SJ, Rowe ML, Howard MJ, Marshall JF, Nissim A (2013) Structural guided scaffold phage display libraries as a source of biotherapeutics. PLoS ONE 8:e70452

Navaratnam V, Fleming KM, West J, Smith CJ, Jenkins RG, Fogarty A, Hubbard RB (2011) The rising incidence of idiopathic pulmonary fibrosis in the U.K. Thorax 66:462–467

Nothelfer EM, Zitzmann-Kolbe S, Garcia-Boy R, Kramer S, Herold-Mende C, Altmann A, Eisenhut M, Mier W, Haberkorn U (2009) Identification and characterization of a peptide with affinity to head and neck cancer. J Nucl Med 50:426–434

Pakkala M, Hekim C, Soininen P, Leinonen J, Koistinen H, Weisell J, Stenman UH, Vepsalainen J, Narvanen A (2007) Activity and

stability of human kallikrein-2-specific linear and cyclic peptide inhibitors. J Pept Sci 13:348–353

Patsenker E, Popov Y, Stickel F, Jonczyk A, Goodman SL, Schuppan D (2008) Inhibition of integrin alphavbeta6 on cholangiocytes blocks transforming growth factor-beta activation and retards biliary fibrosis progression. Gastroenterology 135:660–670

Peng ZW, Ikenaga N, Liu SB, Sverdlov DY, Vaid KA, Dixit R, Weinreb PH, Violette S, Sheppard D, Schuppan D, Popov Y (2016) Integrin alphavbeta6 critically regulates hepatic progenitor cell function and promotes ductular reaction, fibrosis, and tumorigenesis. Hepatology 63:217–232

Pi L, Robinson PM, Jorgensen M, Oh SH, Brown AR, Weinreb PH, Trinh TL, Yianni P, Liu C, Leask A, Violette SM, Scott EW, Schultz GS, Petersen BE (2015) Connective tissue growth factor and integrin alphavbeta6: a new pair of regulators critical for ductular reaction and biliary fibrosis in mice. Hepatology 61:678–691

Puthawala K, Hadjiangelis N, Jacoby SC, Bayongan E, Zhao Z, Yang Z, Devitt ML, Horan GS, Weinreb PH, Lukashev ME, Violette SM, Grant KS, Colarossi C, Formenti SC, Munger JS (2008) Inhibition of integrin alphavbeta6, an activator of latent transforming growth factor-beta, prevents radiation-induced lung fibrosis. Am J Respir Crit Care Med 177:82–90

Raghu G, Collard HR, Egan JJ, Martinez FJ, Behr J, Brown KK, Colby TV, Cordier JF, Flaherty KR, Lasky JA, Lynch DA, Ryu JH, Swigris JJ, Wells AU, Ancochea J, Bouros D, Carvalho C, Costabel U, Ebina M, Hansell DM, Johkoh T, Kim DS, King TE Jr., Kondoh Y, Myers J, Müller NL, Nicholson AG, Richeldi L, Selman M, Dudden RF, Griss BS, Protzko SL, Schünemann HJ; ATS/ERS/JRS/ALAT Committee on Idiopathic Pulmonary Fibrosis (2011) An official ATS/ERS/JRS/ALAT statement: idiopathic pulmonary fibrosis: evidence-based guidelines for diagnosis and management. Am J Respir Crit Care Med 183:788–824

Roxin A, Zheng G (2012) Flexible or fixed: a comparative review of linear and cyclic cancer-targeting peptides. Future Med Chem 4:1601–1618

Saha A, Ellison D, Thomas GJ, Vallath S, Mather SJ, Hart IR, Marshall JF (2010) High-resolution *in vivo* imaging of breast cancer by targeting the pro-invasive integrin alphavbeta6. J Pathol 222:52–63

Saini G, Porte J, Weinreb PH, Violette SM, Wallace WA, McKeever TM, Jenkins G (2015) alphavbeta6 integrin may be a potential prognostic biomarker in interstitial lung disease. Eur Respir J 46:486–494

Satpati D, Hausner SH, Bauer N, Sutcliffe JL (2014) Cerenkov luminescence imaging of alphav beta6 integrin expressing tumors using (90) Y-labeled peptides. J Labelled Comp Radiopharm 57:558–565

Shi J, Wang F, Liu S (2016) Radiolabeled cyclic RGD peptides as radiotracers for tumor imaging. Biophys Rep 2:1–20

Singh AN, McGuire MJ, Li S, Hao G, Kumar A, Sun X, Brown KC (2014) Dimerization of a phage-display selected peptide for imaging of alphavbeta6- integrin: two approaches to the multivalent effect. Theranostics 4:745–760

Ueda M, Fukushima T, Ogawa K, Kimura H, Ono M, Yamaguchi T, Ikehara Y, Saji H (2014) Synthesis and evaluation of a radioiodinated peptide probe targeting alphavbeta6 integrin for the detection of pancreatic ductal adenocarcinoma. Biochem Biophys Res Commun 445:661–666

Utz JP, Ryu JH, Douglas WW, Hartman TE, Tazelaar HD, Myers JL, Allen MS, Schroeder DR (2001) High short-term mortality following lung biopsy for usual interstitial pneumonia. Eur Respir J 17:175–179

Wells AU (2013) Managing diagnostic procedures in idiopathic pulmonary fibrosis. Eur Respir Rev 22:158–162

Win T, Lambrou T, Hutton BF, Kayani I, Screaton NJ, Porter JC, Maher TM, Endozo R, Shortman RI, Lukey P, Groves AM (2012) ^{18}F-Fluorodeoxyglucose positron emission tomography pulmonary imaging in idiopathic pulmonary fibrosis is reproducible: implications for future clinical trials. Eur J Nucl Med Mol Imaging 39:521–528

Xu MY, Porte J, Knox AJ, Weinreb PH, Maher TM, Violette SM, McAnulty RJ, Sheppard D, Jenkins G (2009) Lysophosphatidic acid induces alphavbeta6 integrin-mediated TGF-beta activation via the LPA2 receptor and the small G protein G alpha(q). Am J Pathol 174:1264–1279

Yang GY, Guo S, Dong CY, Wang XQ, Hu BY, Liu YF, Chen YW, Niu J, Dong JH (2015) Integrin alphavbeta6 sustains and promotes tumor invasive growth in colon cancer progression. World J Gastroenterol 21:7457–7467

Yu X, Wu Y, Liu H, Gao L, Sun X, Zhang C, Shi J, Zhao H, Jia B, Liu Z, Wang F (2016) Small-animal SPECT/CT of the progression and recovery of rat liver fibrosis by using an integrin alphavbeta3-targeting radiotracer. Radiology 279:502–512

Zhu X, Li J, Hong Y, Kimura RH, Ma X, Liu H, Qin C, Hu X, Hayes TR, Benny P, Gambhir SS, Cheng Z (2014) ^{99m}Tc-labeled cystine knot peptide targeting integrin alphavbeta6 for tumor SPECT imaging. Mol Pharm 11:1208–1217

